ELSEVIER

Journal of Power Sources 112 (2002) 384–394

JOURNAL OF POWER SOURCES

www.elsevier.com/locate/jpowsour

Preparation and electrochemical properties of Zn-doped $LiNi_{0.8}Co_{0.2}O_2$

G.T.K. Fey[a,*], J.G. Chen[a], V. Subramanian[a], T. Osaka[b]

[a]*Department of Chemical and Materials Engineering, National Central University, Chung-Li 32054, Taiwan, ROC*
[b]*Department of Applied Chemistry, School of Science and Engineering, Waseda University, 3-4-1 Ohkubo, Sinjuku-ku, Tokyo 169-8555, Japan*

Received 22 March 2002; received in revised form 16 July 2002; accepted 25 July 2002

Abstract

Zn-doped $LiZn_yNi_{0.8-y}Co_{0.2}O_2$ ($0.0000 \leq y \leq 0.0100$) compositions were synthesized by a conventional solid-state method. The products were characterized by XRD, galvanostatic cycling, cyclic voltammetry, electrochemical impedance spectroscopy and thermal analysis. For the $LiZn_{0.0025}Ni_{0.7975}Co_{0.2}O_2$ system cycled between 3.0 and 4.2 V, the discharge capacities in the 1st and 100th cycles were 170 and 138 mAh/g with charge retention of 81%. The corresponding values for the undoped material were 158 and 97 mAh/g, with charge retention of 61.4%. The improved electrochemical properties of the doped system were attributed to the structural stability derived from incorporating the size-invariant Zn^{2+} ions. The Zn-doped system also showed improved capacity and cyclability when the cycling was performed in a voltage wider window (2.5–4.4 V) and at a higher temperature (55 °C). The structural and electrochemical properties of the doped and undoped materials were correlated.

Keywords: Lithiated nickel cobalt oxides; $LiNi_{0.8}Co_{0.2}O_2$; Zn-doping; Cathode materials; Lithium ion batteries

1. Introduction

Research into lithium nickel oxide has been gaining momentum because it holds much promise as a cathode material in lithium batteries due to its high practical specific capacity (>150 mAh/g) [1–3], low maximum charging voltage [4] and low cost. Moreover, the chemical potential of lithium in $LiNiO_2$ is lower than in $LiCoO_2$ [5], which makes the contact reduction of $LiNiO_2$ with electrolytes less problematic. However, the commercial exploitation of the material is limited by phase transitions that accompany the charge–discharge processes [1,2]. The resulting deterioration of the crystal structure leads to a high degree of capacity fading [6]. Also, the exothermic decomposition of $LiNiO_2$ in a highly charged state at elevated temperatures (~200 °C) creates safety concerns for the devices that use it [7]. On the other hand, $LiCoO_2$ has been a popular cathode material primarily because of its good reversibility and ease of preparation, but cobalt's cost and toxicity prevent its large-scale use in power sources, especially for consumer applications. Hence, iso-structural solid solutions of the general formula $LiNi_{1-y}Co_yO_2$ have been studied for their electrochemical properties. Because of its improved electrochemical properties, it is now generally recognized that $LiNi_{0.8}Co_{0.2}O_2$ is a potential next-generation cathode material [8–10].

In order to further enhance the electrochemical properties of $LiNi_{0.8}Co_{0.2}O_2$, doping with a number of cations has been carried out and reported to be successful. A partial substitution with Mn in the lithium nickel cobalt oxide matrix resulted in a material with improved structural stability and electrochemical properties [11]. Substitution with Al was also found to improve the capacity of the host, but did not improve the safety characteristics [12]. A partial substitution with Ti and Mg for Ni in $LiNi_{0.8}Co_{0.2}O_2$ resulted in excellent cycling stability and safety characteristics [12]. Similar results of improved capacity and safety characteristics for the Mg-doped $LiNi_{0.75}Co_{0.25}O_2$ were reported [13]. Cho [10] reported the electrochemical properties of $LiNi_{0.74}Co_{0.26-y}Mg_yO_2$. Recently, we reported the effect of partially substituting Ni in $LiNi_{0.8}Co_{0.2}O_2$ with Ti and Mg/Al/Zn [14]. Chowdari et al. [15] have studied the cathodic properties of (Co, Ti, and Mg)-doped $LiNiO_2$. Mg-doped lithium nickel cobalt oxides were studied for their

* Corresponding author. Tel.: +886-3-425-7151x4206; fax: +886-3-425-7325.
E-mail address: gfey@cc.ncu.edu.tw (G.T.K. Fey).

0378-7753/02/$ – see front matter
PII: S0378-7753(02)00400-7

cycling behavior in a 4/5 'A' size cylindrical cell. The system showed cycling stability over more than 500 cycles [16]. Electrochemical properties of $LiNi_{0.85}Co_{0.10}M_{0.05}O_2$ in which part of the Ni was replaced with Al or Fe were also recently reported [17].

Mg-doped $LiNiO_2$ and $LiNi_{1-y}Co_yO_2$ [10,12,16] and Al-doped $LiCoO_2$ [18,19] have also been investigated extensively for their cathodic and safety characteristics. Thus, electro-inactive non-transition metal ions, particularly Mg^{2+} and Al^{3+}, have been of great interest as dopants for cathode materials. However, to the best of our knowledge, another potential non-transition metal ion, Zn^{2+}, has not received as much attention as a dopant for layered cathode materials. In this paper, we report the effects of doping with Zn on the structural and electrochemical properties of the $LiNi_{0.8}Co_{0.2}O_2$ system. The cycling behavior in different voltage windows as well as at 25 and 55 °C was studied. The changes in the electrochemical characteristics of the material upon doping are explained with the results of our cyclic voltammetric and electrochemical impedance studies. The safety characteristics of the doped materials in their fully charged states were studied using differential scanning calorimetry.

2. Experimental

$LiZn_yNi_{0.8-y}Co_{0.2}O_2$ compositions, where $y = 0.0000$, 0.0010, 0.0025, 0.0050, 0.0075, and 0.0100, were synthesized by a solid-state method from stoichiometric amounts of $LiOH{\cdot}H_2O$, NiO, Co_3O_4, and ZnO. However, a slightly excess stoichiometry of lithium (1.05) was used to compensate for any loss of the metal that might have occurred during the firing at high temperatures. The appropriate stoichiometric amounts of the chemicals were ground in an agate mortar, pressed into pellets, and fired at 800 °C for 20 h in flowing oxygen at a heating ramp of 250 °C/h. The products were cooled to 500 °C at 60 °C/h, then to room temperature by natural convection, and ground to a fine polycrystalline powder.

X-ray diffraction patterns were recorded on a Siemens D-5000 diffractometer between diffraction angles of 5 and 80° in increments of 0.05°. Chemical analysis of the synthesized materials was performed with an inductively coupled plasma–atomic emission spectrometer (Kontron, NS-35 ICP–AES). The elemental analysis was done to confirm the stoichiometry of the products. As can be seen from Table 1, the results of the elemental analysis agree well with the targeted compositions. The small loss in lithium content from the initial stoichiometry represents the lithium lost during the calcination treatment.

Electrochemical studies were performed on 2032-type coin cells with lithium metal as the anode. The electrolyte used was 1 M $LiPF_6$ in 50:50 EC/DEC (v/v) (Tomiyama Chemicals). All manipulations were performed in an argon-filled glove box (VAC MO40-1) in which the oxygen and moisture levels were below 3 and 10 ppm, respectively. The electrochemical cycling was performed in a galvanostatic mode at a 0.1 C rate in a multi-channel battery cycling unit (Maccor, 4000 Series) interfaced with an IBM PC. The cathodes were prepared by slurry-coating a mixture of the active material (85%), carbon black (10%), and PVdF (5%) in NMP on to an aluminum foil, drying the coating overnight at 120 °C in an oven, roller-pressing, and punching circular discs from the foil.

Cyclic voltammetry was performed in a three-electrode glass cell placed inside the glove box. The cathode materials were prepared as described, but coated on both sides of the aluminum foil. The anode and electrolyte were the same as the ones used for the coin cells. The cyclic voltammetric experiments were run on a Solartron 1287 electrochemical interface at a scan rate of 100 μV/s between 2.5 and 4.4 V. The ac impedance spectra at different depths of charge and discharge were recorded with the coin cells. The impedance behavior was studied between 65 and 0.001 Hz with a Solartron 1250/1287 set up, and analyzed using Z-view software from Scribner Associates. The cells were galvanostatically charged and discharged to record the impedance spectra at various depths of intercalation and deintercalation.

For the thermal characterization of the materials, the coin cells were first galvanostatically charged to 4.4 V at a 0.1 C rate and then potentiostated at 4.4 V for 20 h in a multi-channel battery tester (Maccor 4000). During this period, the current dropped to microampere levels. After 20 h, the coin cells were opened inside the glove box in which the oxygen and moisture content were less than 2 ppm. The cathode of the coin cell was carefully removed and the excess electrolyte was wiped with a Kimwipes® cloth. All the recovered materials had 10–15% electrolyte by weight. The material

Table 1
Results of ICP–AES analysis of the undoped and Zn-doped $LiNi_{0.8}Co_{0.2}O_2$

Synthesized composition y in $LiZn_yNi_{0.8-y}Co_{0.2}O_2$	ICP–AES analysis, composition (%)				Suggested formula
	Li	Ni	Co	Zn	
0.0000	7.20	44.9	12.0	0	$Li_{1.04}Ni_{0.77}Co_{0.20}O_{1.98}$
0.0010	7.18	46.1	12.1	0.056	$Li_{1.03}Zn_{0.00086}Ni_{0.79}Co_{0.21}O_{2.02}$
0.0025	7.21	46.3	11.8	0.157	$Li_{1.04}Zn_{0.0024}Ni_{0.79}Co_{0.20}O_{2.00}$
0.0050	7.19	45.3	12.0	0.294	$Li_{1.04}Zn_{0.0045}Ni_{0.77}Co_{0.20}O_{1.98}$
0.0075	7.24	45.6	11.4	0.464	$Li_{1.04}Zn_{0.0071}Ni_{0.77}Co_{0.19}O_{1.97}$
0.0100	7.27	46.7	12.1	0.647	$Li_{1.05}Zn_{0.0098}Ni_{0.80}Co_{0.21}O_{2.05}$

was carefully removed from the aluminum current collector and loaded on to an aluminum pan. The aluminum pan was hermetically sealed, placed in an airtight container, and immediately transferred to a DSC instrument (Perkin-Elmer DSC 7) for measurements. The DSC experiments were carried out between 150 and 350 °C at a heating rate of 3 °C/min in a nitrogen atmosphere.

3. Results and discussion

3.1. Structural properties

The typical X-ray diffraction patterns recorded for the undoped and Zn-doped (0.0025) materials are shown in Fig. 1. All the diffractograms show patterns indexable in the α-$NaFeO_2$ layered structure assuming a hexagonal lattice setting. The diffraction patterns show a clear splitting of the hexagonal characteristic doublets (0 0 6)/(1 0 2) and (1 0 8)/(1 1 0). This indicates that the products possessed typical layered characteristics. The hexagonal unit cell parameters calculated for all the products are in agreement with literature values [8]. The *c*/*a* ratio initially increases with an increase in the Zn-dopant concentration and then levels off. The ratio of the intensity of the (0 0 3) reflection to that of the (1 0 4) reflection increases up to a dopant level of 0.0025 and then decreases. The decrease in the peak intensity ratio has a direct impact on the electrochemical properties of the system. It has been used as an indicator for cation mixing in the case of doped layered structures [20]. Values lower than 1.3 indicate a high degree of cation mixing, due primarily to the occupancy of dopant ions in the lithium interslab region. The *R*-factor, defined by Reimers et al. [21] as $[I_{006} + I_{102}]/I_{101}$, is considered a good indicator of hexagonal ordering of the system. The lower the *R*-factor of a system, the higher the hexagonal ordering. In the present study, the *R*-factor was the lowest for the system with $y = 0.0025$ in $LiZn_yNi_{0.8-y}Co_{0.2}O_2$. Fig. 2 shows the variation of the *R*-factor as a function of the dopant concentration. The minimum in the value for the *R*-factor shows that at a *y*-value of 0.0025, the system exhibits the maximum hexagonal ordering. A good hexagonal ordering of the layered structures means a good ordering of the 3b lithium ion sites and the 3a transition metal ion sites.

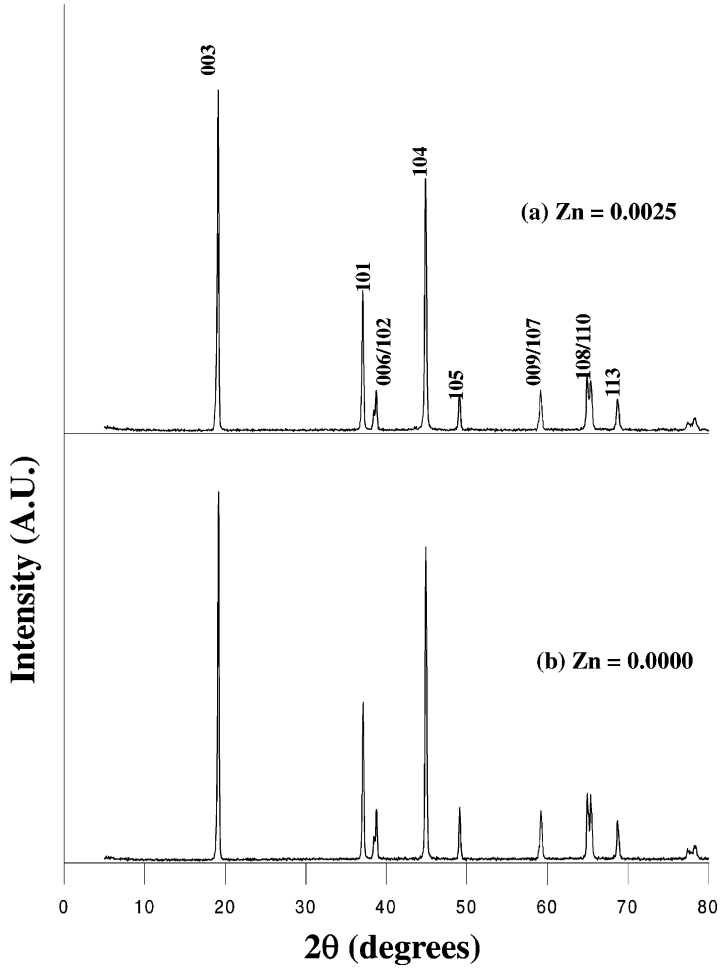

Fig. 1. Typical X-ray diffractograms of $LiZn_yNi_{0.8-y}Co_{0.2}O_2$ ($y = 0.0025$) and $LiNi_{0.8}Co_{0.2}O_2$.

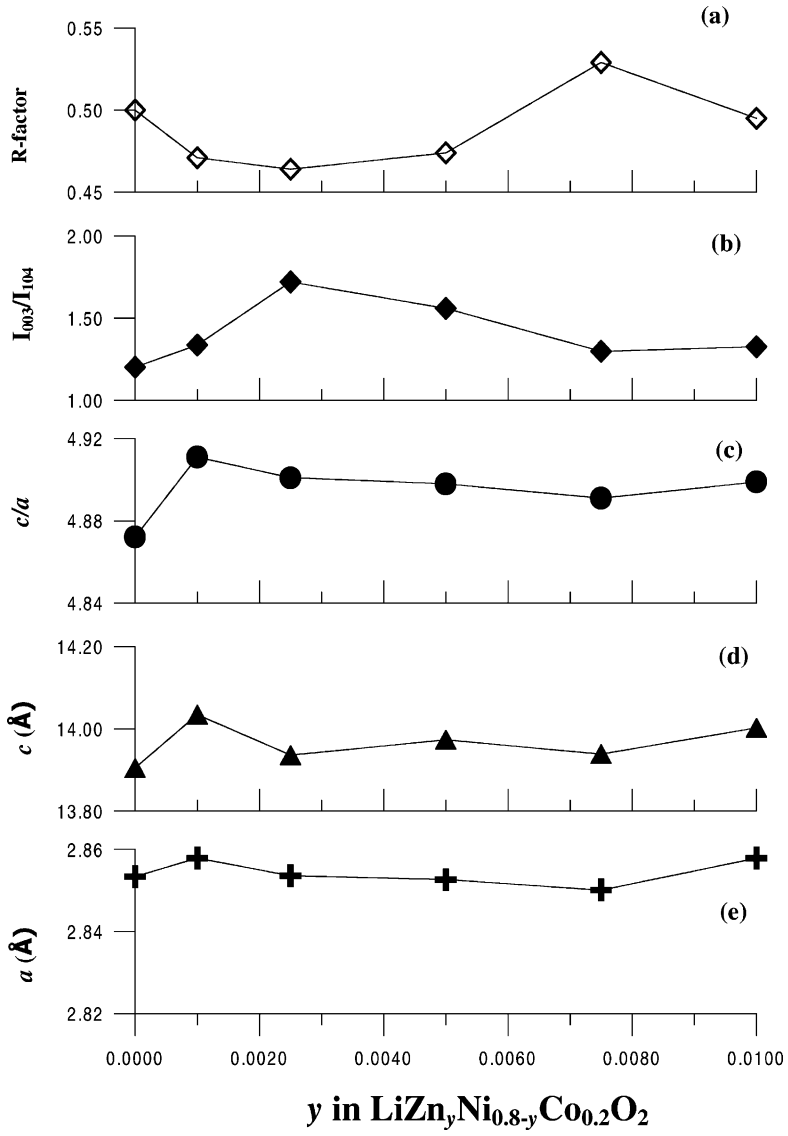

Fig. 2. Variation of lattice constants and other crystallochemical parameters as a function of the Zn-dopant concentration.

3.2. Charge–discharge studies

3.2.1. Cycling studies at 25 °C

The cycling performance of the undoped as well as the Zn-doped $LiNi_{0.8}Co_{0.2}O_2$ materials in the voltage range 3.0–4.2 V at 25 °C are shown in Fig. 3. The discharge capacities in the 1st and 10th cycles for $LiNi_{0.8}Co_{0.2}O_2$ were 158 and 153 mAh/g, respectively, with charge retention of 96%. The capacity in the 100th cycle was 97 mAh/g, corresponding to charge retention of 61.4%. At $y = 0.0010$, there was no change in the initial capacity, although the capacity in the 10th cycle was a much lower 129 mAh/g. However, when the dopant level was increased to 0.0025, an enhancement in capacity as well as cyclability was observed. The 1st, 10th and the 100th cycle capacities were 170, 168, and 138 mAh/g, recording charge retention of 99 and 81% in the 10th and the 100th cycles, respectively. A further increase in the Zn content led to a decrease in both the capacity and the cyclability as shown in Fig. 3.

The increase in the cycling stability of the Zn-doped systems, as observed in all the compositions studied, can be attributed to the presence of the size-invariant Zn^{2+} ions in the interslab regions of the products [22]. From the ionic radii for a six-coordination (Li^+, 0.76 Å; Ni^{2+}, 0.69 Å; Ni^{3+}, 0.56 Å; Co^{2+}, 0.64 Å; Co^{3+}, 0.545 Å; Zn^{2+}, 0.88 Å) [23], one can reasonably assume that the Zn-dopant will occupy the lithium sites instead of the transition metal sites. From a general point of view, layered-type $LiMO_2$ compounds are formed because of the size differences between [LiO_6] and [MO_6] octahedra. Therefore, the larger Zn cations are expected to preferentially occupy the lithium sites if the Li/M ratio is less than 1. According to Gao et al. [20], a value of more than 1.3 for the I_{003}/I_{104} intensity ratio is an indicator of reduced cation mixing. Thus, it looks possible

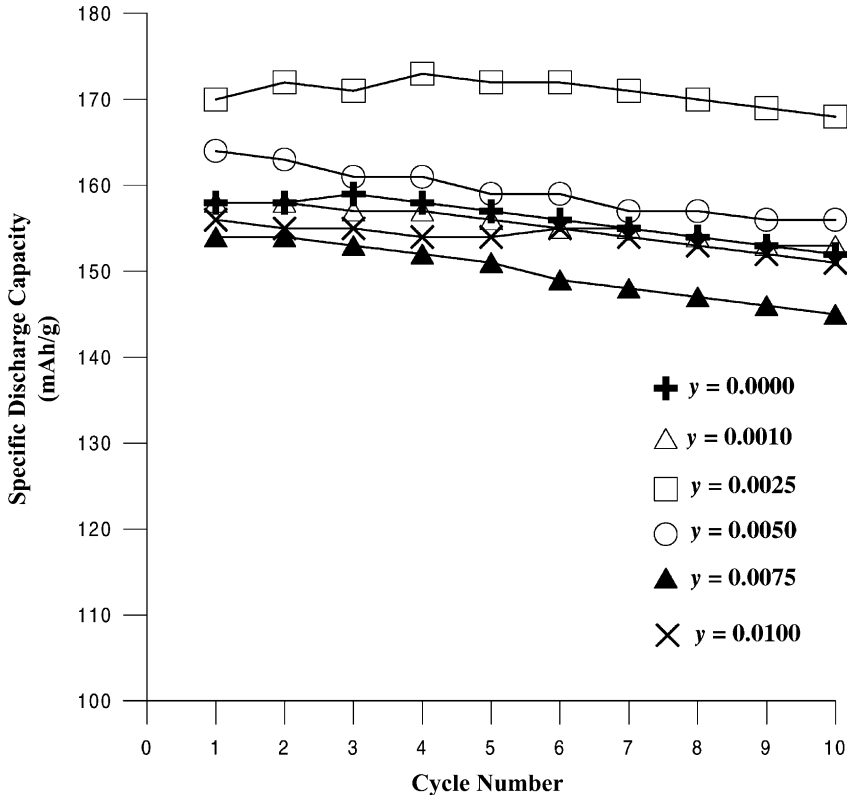

Fig. 3. Cycling performance of the various $LiZn_yNi_{0.8-y}Co_{0.2}O_2$ compositions at 25 °C. Voltage range: 3.0–4.2 V.

that a part of the dopant ions reside in the interslab spaces. By a magnetic susceptibility study, Pouillerie et al. [24] confirmed the presence of Mg^{2+} ions (ionic radius 0.72 Å [23]) in the interslabs of $LiMg_yNi_{1-y}O_2$. We have extended their results to support the possible presence of Zn^{2+} in the interslabs in Zn-doped $LiNi_{0.8}Co_{0.2}O_2$. The presence of the size-invariant Zn^{2+} ions in the interslab region prevents structural transformations during the topotactic reactions, enhancing the cyclability of the system.

In the case of $LiMO_2$ systems doped with a divalent non-transition metal ion, the capacity of the doped system is expected to be lower than that of the undoped one because of the attendant oxidation of the electrochemically active trivalent M ions to its 4 V inactive tetravalent form in order to maintain the charge balance. In fact, for every fraction of the trivalent ion that is replaced, an equivalent amount is oxidized, thereby reducing the amount of the electroactive trivalent M species by twice the divalent dopant concentration. However, in the present case, introducing the divalent Zn led to an increase in capacity and cyclability of the system. Although the dopant concentrations were too low to warrant a noticeable loss in capacity, the increase in capacity is rather unusual. The reason for this atypical behavior is not immediately clear.

Having identified that the composition with a dopant stoichiometry of 0.0025 was the best-performing material, a comparative study of the cycling behavior of the material with that of the undoped one was made in a wider voltage window, between 2.5 and 4.4 V. The first discharge capacities for the undoped and the Zn-doped ($y = 0.0025$) $LiNi_{0.8}Co_{0.2}O_2$ were 175 and 182 mAh/g, respectively. The values of the charge retention in the 10th cycle for the two materials were 91 and 93%, respectively. Our results show that at a doping level of 0.0025, Zn improves both the capacity and cyclability of $LiNi_{0.8}Co_{0.2}O_2$.

3.2.2. Cycling performance at 55 °C

Doping with non-transition metal ions is generally believed to impart structural stability to the host matrix during topotactic reactions. In order to further investigate this effect, the cycling was performed at 55 °C for both the undoped and Zn-doped ($y = 0.0025$) systems between 3.0 and 4.2 V at a 0.1 C rate. $LiNi_{0.8}Co_{0.2}O_2$ gave a first-cycle discharge capacity of 184 mAh/g, which was a dramatic improvement over the 158 mAh/g it delivered at 25 °C. However, the improvement in the first-cycle capacity for the Zn-doped system at the higher temperature was only marginal, from 170 to 178 mAh/g. Although, the elevated-temperature performance of the Zn-doped material was inferior to that of the undoped material, the general improvement in the performance of the materials with an increase in the temperature may be attributed to the increased diffusion of lithium ions at the higher temperature. Recently, Van der Ven and Ceder [25,26], based on a theoretical analysis,

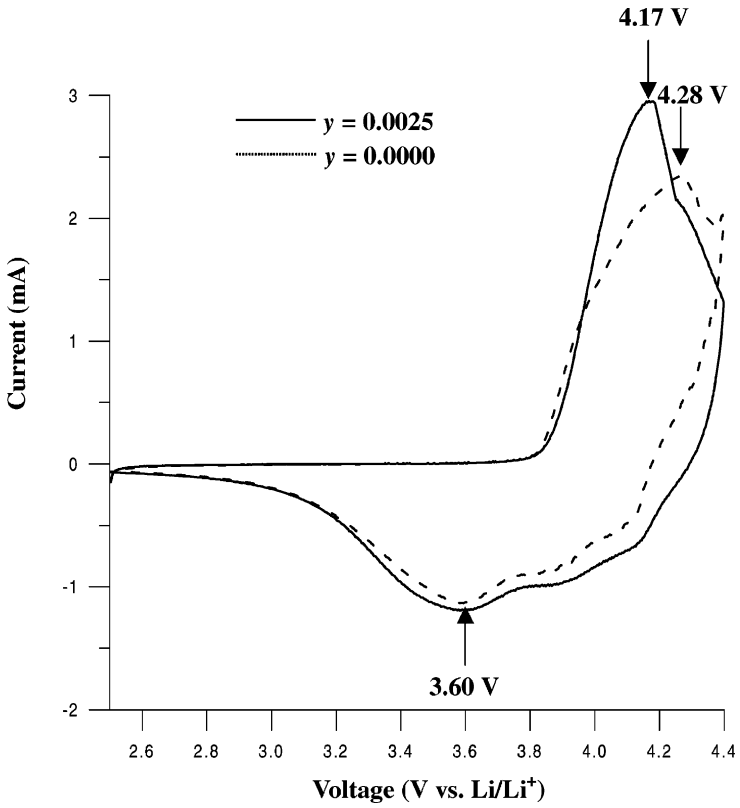

Fig. 4. Cyclic voltammograms of $LiNi_{0.8}Co_{0.2}O_2$ and $LiZn_yNi_{0.8-y}Co_{0.2}O_2$ ($y = 0.0025$). Scan rate: 0.1 mV/s.

showed that the capacity and electrochemical properties of O3-type oxides were mainly determined by the diffusion of lithium ions in the oxide matrix. Although the doped system showed a lower first-cycle discharge capacity at 55 °C, its cycling stability was superior to that of the undoped system. The charge retention of the former in the 30th cycle was 94%, while that of the latter was a diminished 89%. This is further proof that doping with non-transition metal ions improves cycling stability. In our case, doping with very small quantities of Zn resulted in improved capacity and cycling stability both at room and elevated temperatures.

3.3. Cyclic voltammetric studies

Cyclic voltammograms recorded for the undoped as well as the Zn-doped ($y = 0.0025$) $LiNi_{0.8}Co_{0.2}O_2$ systems are shown in Fig. 4. For the undoped system, the deintercalation and intercalation processes occurred at 4.28 and 3.6 V, respectively. Doping with Zn advanced the deintercalation potential to 4.17 V, an indication that the overpotential for the deintercalation process was reduced. The reduced difference between the potentials of the two processes further shows a greater reversibility for the electrode processes upon Zn-doping. The higher currents associated with the Zn-doped system indicate the higher capacity deliverable from the doped system. The large deintercalation currents seen in the cyclic voltammograms agree with the first-cycle charge and discharge capacities for the respective materials. For example at 25 °C, they were 193 and 175 mAh/g, respectively, for the undoped material, and 213 and 182 mAh/g, respectively, for the Zn-doped material. The large first-cycle irreversibility of the materials is reflected in the cyclic voltammograms.

3.4. Electrochemical impedance spectroscopic studies

The impedance spectra recorded at different depths of charge and discharge for the Zn-doped ($y = 0.0025$) and the undoped $LiNi_{0.8}Co_{0.2}O_2$ systems are shown in Fig. 5. According to Levi et al. [27], the high-frequency semicircle is related to the surface film, the medium-to-intermediate frequency semicircle to the charge transfer process and the interfacial capacitance, and the low-frequency tail to the diffusion of lithium ions in the bulk active mass. Similar impedance patterns were observed for spinel $LiMn_2O_4$ as well as for other layered systems [27,28]. In the case of $LiNi_{0.8}Co_{0.2}O_2$ (Fig. 5c and d), the diameter of the first semicircle did not seem to have any significant dependence on the potential, both during charging and discharging, signifying that the film formation process is independent of the lithium content. On the other hand, the charge transfer resistance, R_{ct}, showed a greater dependence on the lithium intercalation and deintercalation levels (i.e. on the voltage at which the impedance measurements were made). In the highly charged states, the material was found to give the lowest values for R_{ct}. The reduced values for R_{ct} are a result

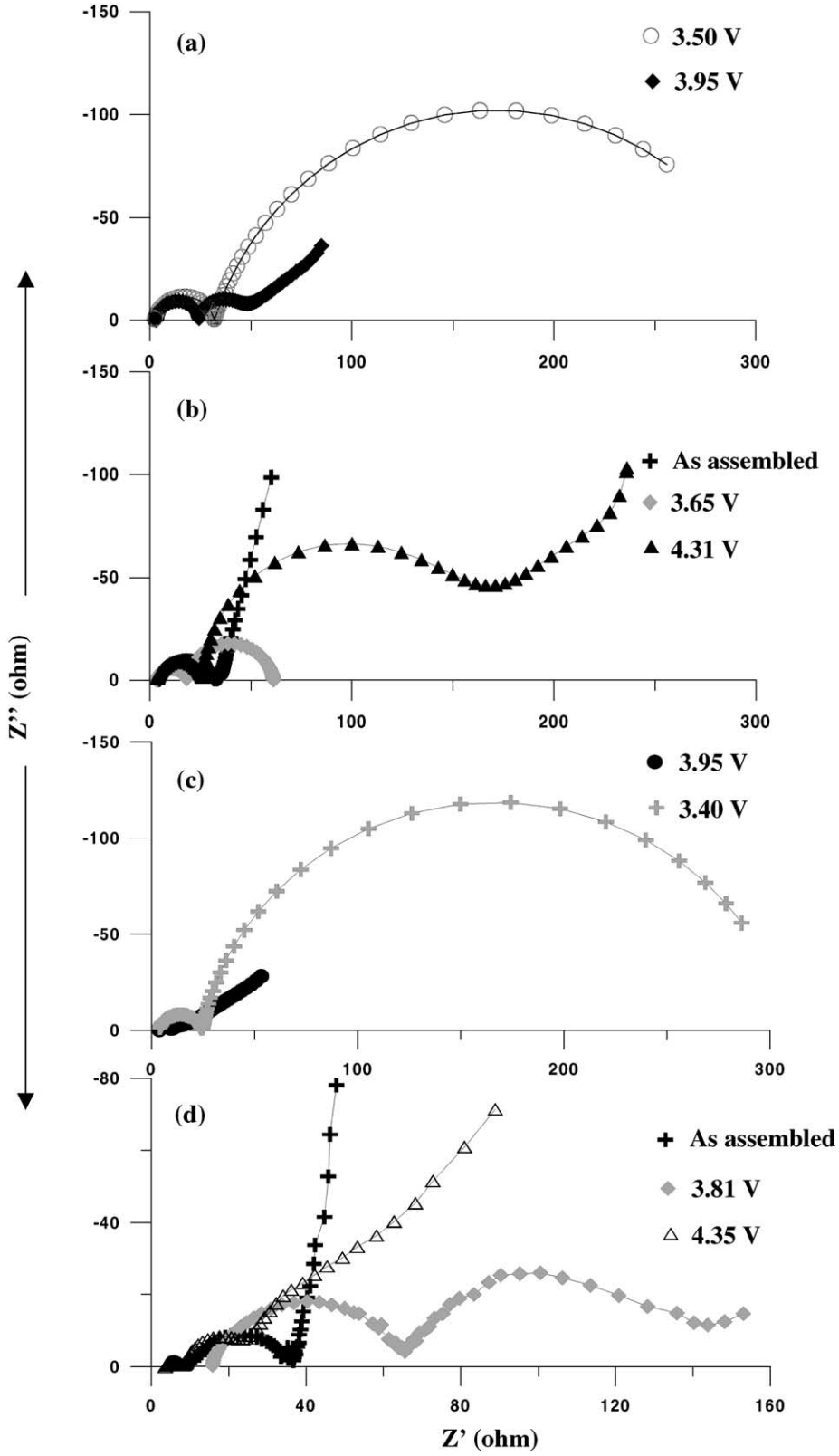

Fig. 5. EIS spectra of the various $LiZn_yNi_{0.8-y}Co_{0.2}O_2$ compositions recorded during first charge and discharge at different voltages: (a) $y = 0.0025$, on discharge; (b) $y = 0.0025$, on charge; (c) $y = 0.0000$, on discharge; and (d) $y = 0.0000$, on charge.

of the material turning more conductive at the reduced lithium levels. As more and more lithium is removed from the lattice, the lattice expands because of the increased electrostatic repulsion between the negatively charged oxygen layers, facilitating easier lithium diffusion into the matrix. This behavior, as can be seen from Fig. 5c and d, is consistent with the results of Corse et al. [28]. However, according to Levi et al. [27] there is an initial decrease in the charge transfer resistance upon deintercalation, followed by a considerable increase in the fully charged state.

The Nyquist plots recorded for the Zn-doped system are shown in Fig. 5a and b. Despite their very low levels, dopants resulted in significant differences in the impedance behavior. The R_{ct}-value for the fully charged system was higher than for the partially charged system, which is in agreement with the observations of Levi et al. [27]. Levi et al. [27] attribute the increase in R_{ct} as the deintercalation progresses to an increased disorder of the outer particle layer in contact with the surface layer. A tentative explanation for the different impedance behavior of the Zn-doped material is provided below. According to Pouillerie et al. [16,22], who investigated the effect of Mg-doping in $LiNiO_2$ and $LiCo_yNi_{1-y}O_2$, all the Mg^{2+} ions migrated from the slabs to the interslab region in the first cycle. If the Zn ions similarly migrate to the interslab region in the first cycle, they may account for the increase in the charge transfer resistance observed in our studies. The presence of the Zn ions in the lithium interplane has a direct influence on the diffusion of lithium. The presence of the size-invariant Zn ions in the lithium interslab is also believed to improve the cycling stability of the system. However, the increase in R_{ct} as the lithium deintercalation level increased was not restricted to the first cycle alone, as the trend continued in the impedance patterns of the sample in the second and third cycles too. The resistances associated with the different processes during intercalation and deintercalation were calculated using equivalent circuit modeling, as discussed below.

The complex processes occurring during intercalation and deintercalation are difficult to understand. It is more convenient to describe them with the equivalent circuit models shown in Fig. 6. The impedance parameters derived are summarized in Tables 2 and 3. Model 1 Fig. 6a) is a simple combination of resistances, a constant phase element (CPE) and Warburg impedance. In Model 2 Fig. 6b), there are two CPEs laid parallel with resistances, particle-to-particle resistance (R_p) and charge transfer resistance (R_{ct}). The equivalent circuit shown in Fig. 6c was proposed by Choi et al. [29]. The term R_e in the equivalent circuit is the electrolyte resistance. The constant phase elements, CPE 1 and 2, are used to account for the depressed semicircles in the Nyquist

Table 2
Impedance parameters derived using equivalent circuit models for $LiNi_{0.8}Co_{0.2}O_2$

Voltage (V)	R_e [a] (Ω)	R_p [a] (Ω)	R_{ct} [a] (Ω)	CPE 1 [b] (F)		CPE 2 [b] (F)		Z_W [c] (Ω)		
				T ($\times 10^{-5}$)	P	T	P	R	T	P
As assembled (2.80) [d]	9.796	25.000	–	1.908	0.777	–	–	6.1	0.06	0.446
Partially charged (3.81) [e]	14.710	52.400	78.0	3.326	0.747	0.0081	0.769	–	–	–
Fully charged (4.35) [f]	5.669	4.062	9.2	4.572	0.799	0.0255	1.140	190.9	1003.00	0.429
Partially discharged (3.95) [f]	3.756	6.100	3.8	1.712	0.850	0.0083	0.980	241.1	5777.00	0.460
Fully discharged (3.40) [d]	4.530	21.300	278.0	3.450	0.748	0.1325	0.909	–	–	–

[a] R_e: electrolyte resistance; R_p: particle-to-particle resistance; R_{ct}: charge transfer resistance.
[b] Capacitance for CPE: constant phase element; T and P are the constant phase parameters of the equation $Z = 1/[T(I^*\omega)^P]$, used for fitting the depressed semicircles in the Nyquist plots ($*$ represents the complex conjugate $I = \sqrt{-1}$; ω is the angular frequency of the ac signal).
[c] P, R, T are the Warburg (W) parameters of the equation $Z = R^*\,\mathrm{ctnh}([I^*T^*\omega]^P)/(I^*T^*\omega)^P$ use for fitting the low-frequency straight line of the Nyquist plots.
[d] Calculated using Model 1 [Fig. 6a].
[e] Calculated using Model 2 [Fig. 6b].
[f] Calculated using Model 3 [Fig. 6c].

Table 3
Impedance parameters derived using equivalent circuit models for $LiZn_yNi_{0.8-y}Co_{0.2}O_2$ ($y = 0.0025$)

Voltage (V)	R_e (Ω)	R_p (Ω)	R_{ct} (Ω)	CPE 1 (F)		CPE 2 (F)		Z_W (Ω)		
				T ($\times 10^{-5}$)	P	T	P	R	T	P
As assembled (2.90) [a]	4.000	28.000	–	2.076	0.741	–	–	8.25	8	0.420
Partially charged (3.65) [b]	3.255	15.000	43.0	1.926	0.841	0.009	0.880	–	–	–
Fully charged (4.31) [c]	3.355	23.000	126.0	1.925	0.856	0.009	0.983	288	555	0.512
Partially discharged (3.95) [c]	3.086	21.250	20.0	0.533	0.915	0.009	0.930	125	900	0.440
Fully discharged (3.50) [b]	2.370	29.500	280.0	0.500	0.840	0.083	0.803	–	–	–

[a] Calculated using Model 1 [Fig. 6a].
[b] Calculated using Model 2 [Fig. 6b].
[c] Calculated using Model 3 [Fig. 6c].

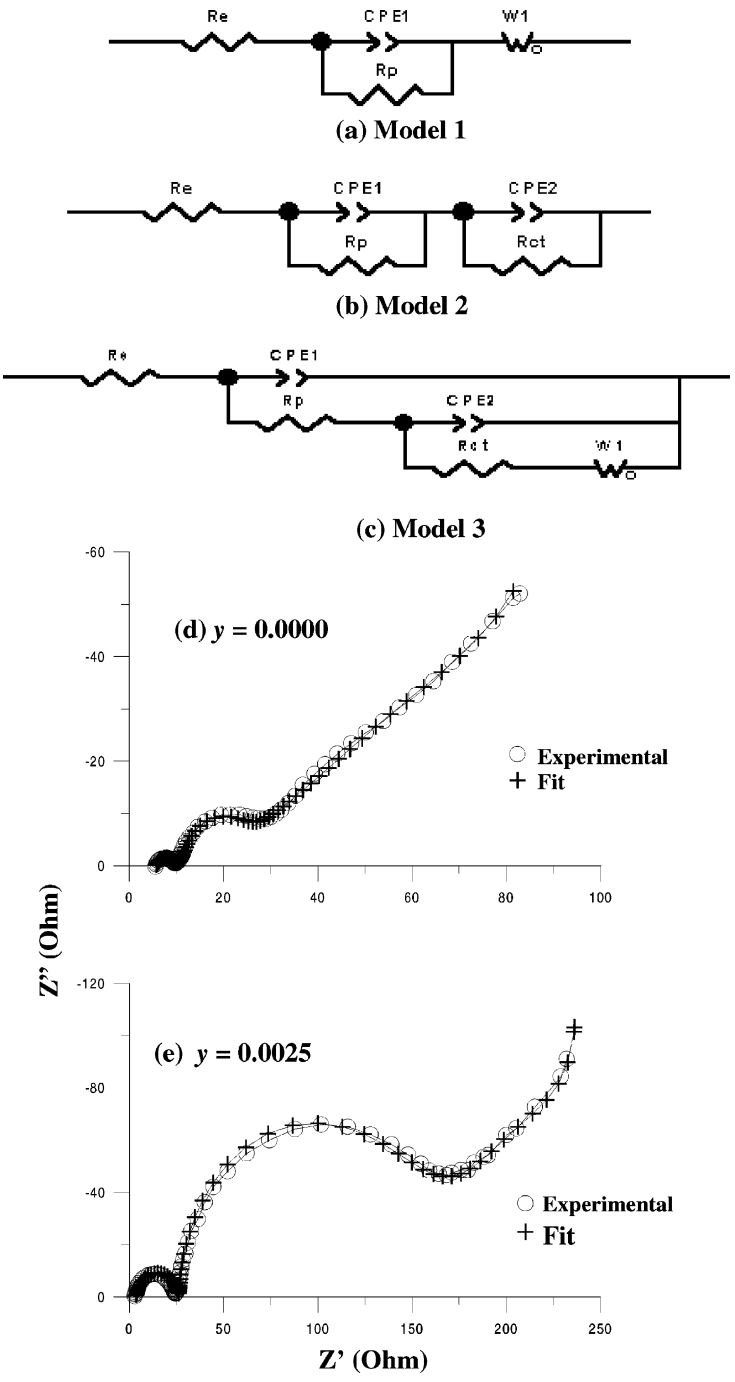

Fig. 6. Equivalent circuit models used in the present study and the experimental and simulated curves using Model 3 for $LiNi_{0.8}Co_{0.2}O_2$ and $LiZn_yNi_{0.8-y}Co_{0.2}O_2$ ($y = 0.0025$) in their fully charged states. (a) Model 1; (b) Model 2; (c) Model 3; (d) $LiNi_{0.8}Co_{0.2}O_2$; and (e) $LiZn_yNi_{0.8-y}Co_{0.2}O_2$ ($y = 0.0025$).

plots [29] that arise from the complicated electrochemical phenomena taking place during the intercalation–deintercalation reactions. Although there is no direct evidence of any deposit of Zn on the grain boundaries, the variation of R_p as a function of the state-of-charge of the doped material shows that R_p is at its highest value at the lowest states-of-charge and reaches a minimum in the fully charged state. This may suggest a possible scavenging of lithium by any accumulated surface Zn, with the increase in the R_p being related to the increased resistance provided by subsequent extensive passivation.

Typical fit plots arrived at by using Model 3 Fig. 6c) are shown in Fig. 6d and e. As can be seen from Tables 2 and 3, the variance of charge transfer resistance with increasing deintercalation changed when Zn was introduced as a dopant in $LiNi_{0.8}Co_{0.2}O_2$. The impedance spectra of the partially charged and discharged $LiNi_{0.8}Co_{0.2}O_2$ show a negligible Warburg tail, an indication that the charge transfer processes

Table 4
Thermal history of $LiZn_yNi_{0.8-y}Co_{0.2}O_2$ compositions in their fully charged states

System (y)	Decomposition temperature (°C)	Exothermic enthalpy (J/g)
0.0000	221	62
0.0025	218	55
0.0100	223	51

overlapped with the lithium diffusion process. As expected for a battery system in which the electrolyte does not take part in the charge–discharge processes, the solution resistance is independent of the voltage at which the measurements were made. The capacitances associated with the surface film are of the order of microfarads (Tables 2 and 3), as observed by other workers [30]. Similarly, the capacitances associated with the charge transfer process are of the order of several hundreds of millifarads [30], as our results reveal (Tables 2 and 3). Fig. 6d and e show that the experimental values agree with those derived with Model 3.

3.5. Thermal stability studies

Differential scanning calorimetry runs were made with $LiNi_{0.8}Co_{0.2}O_2$ and its Zn-doped counterparts ($y = 0.0025$ and 0.0100) in their fully charged states, in order to study their thermal stability characteristics. At a heating rate of 3 °C/min, the major exothermic reactions of lithium nickel cobalt oxide materials occur around 220 °C [10,15]. In the present study, $LiNi_{0.8}Co_{0.2}O_2$ was found to decompose at 221 °C, the associated exothermic enthalpy being 62 J/g (Table 4). There was a decrease in both the decomposition temperature (218 °C) and the enthalpy (55 J/g) when the Zn-dopant level was 0.0025. A similar reduction in decomposition temperature was brought about by Mg-doping, as observed by Lee et al. [17] in their studies with Mg-doped $LiNi_{0.74}Co_{0.26}O_2$. When the Zn-dopant level was increased to 0.0100, the enthalpy value decreased further to 51 J/g, although the decomposition temperature was 223 °C. Hence, a Zn-dopant level of 0.0025 not only yielded good charge–discharge characteristics, but also imparted a certain degree of thermal stability to $LiNi_{0.8}Co_{0.2}O_2$.

4. Conclusions

Undoped and Zn-doped $LiNi_{0.8}Co_{0.2}O_2$ compositions were synthesized by a solid-state method. X-ray diffraction patterns revealed single-phase compounds with all peaks indexable in the R-3m space group. The $I_{0\,0\,3}/I_{1\,0\,4}$ peak intensity ratios for all the compounds were well above 1, which indicates that there was no cation mixing. The charge–discharge properties of the system were studied between 3.0 and 4.2, and 3.0 and 4.4 V at 25 and 55 °C. The 1st and 100th discharge capacities for $LiNi_{0.8}Co_{0.2}O_2$ were 158 and 97 mAh/g, respectively, in the voltage region between 3.0 and 4.2 V at 25 °C. The corresponding values for the best Zn-doped material in the present study ($y = 0.0025$), were 170 and 138 mAh/g. Both the materials gave enhanced capacities at 55 °C, the undoped one a first-cycle capacity of 184 mAh/g, and the doped one 178 mAh/g. When cycled between 2.5 and 4.4 V at 25 °C, the first discharge capacities were 175 and 182 mAh/g for the undoped and the doped systems, respectively. In all the above studies, the cycling efficiency for the doped system ($y = 0.0025$) was higher than that for the undoped system, which indicates that doping $LiNi_{0.8}Co_{0.2}O_2$ with a small but optimal amount of Zn not only enhances the capacity but also the cyclability of the host. The reversibility of the redox processes was supported by the cyclic voltammetry studies. EIS studies performed at different charging and discharging voltages showed a decrease in the charge transfer resistance as lithium was removed from the $LiNi_{0.8}Co_{0.2}O_2$ matrix. However, in the case of the Zn-doped system, there was an unusual increase in the charge transfer resistance in a fully charged state. Equivalent circuit models were proposed to fit the experimental data. The thermal stability of the doped and undoped systems was studied using DSC. At a Zn-dopant concentration of $y = 0.0025$, the decomposition temperature was 218 °C versus 221 °C for the undoped compound. The enthalpy associated with the decomposition processes was found to be the lowest for the system with the highest Zn concentration.

Acknowledgements

Financial support by the National Science Council of the Republic of China is gratefully acknowledged (NSC-90-2214-E-008-003). One of the authors (V. Subramanian) thanks the National Science Council for the award of a post-doctoral fellowship.

References

[1] T. Ohzuku, A. Ueda, M. Nagayama, J. Electrochem. Soc. 140 (1993) 1862.
[2] W. Li, J.N. Reimers, J.R. Dahn, Solid State Ionics 67 (1993) 123.
[3] H. Arai, S. Okada, H. Ohtsuka, M. Ichimura, J. Yamaki, J. Solid State Ionics 80 (1995) 261.
[4] R.V. Moshtev, P. Zlatilova, V. Manev, A. Sato, J. Power Sources 54 (1995) 329.
[5] T. Ohzuku, A. Ueda, M. Nagayama, Y. Iwakoshi, H. Komori, Electrochim. Acta 38 (1993) 1159.
[6] C.C. Chang, P.N. Kumta, J. Power Sources 75 (1998) 44.
[7] T. Ohzuku, A. Ueda, Solid State Ionics 69 (1994) 201.
[8] C. Delmas, I. Saadoune, A. Rougier, J. Power Sources 43/44 (1993) 595.
[9] J. Aragane, K. Matsui, H. Andoh, S. Suzuki, F. Fukuda, H. Ikeya, K. Kitaba, R. Ishikawa, J. Power Sources 68 (1997) 13.
[10] J. Cho, Chem. Mater. 12 (2000) 3089.
[11] M. Yoshio, H. Noguchi, J. Itoh, M. Okada, T. Mouri, J. Power Sources 90 (2000) 176.

[12] Y. Gao, M. Yakovleva, E. Ebner, A. Quinn, R. Schwindeman, B. Fitch, J. Engel, Electrochemical Society, Fall Meeting, Boston, USA, 1998.
[13] C.C. Chang, J.Y. Kim, P.N. Kumta, J. Power Sources 89 (2000) 56.
[14] V. Subramanian, G.T.K. Fey, Solid State Ionics 148 (2002) 351.
[15] B.V.R. Chowdari, G.V. Subba Rao, S.Y. Chow, Solid State Ionics 140 (2001) 55.
[16] C. Pouillerie, F. Perton, Ph. Biensan, J.P. Peres, M. Brousseley, C. Delmas, J. Power Sources 96 (2001) 293.
[17] K.K. Lee, W.S. Yoon, K.B. Kim, K.Y. Lee, S.T. Hong, J. Power Sources 97/98 (2001) 308.
[18] S. Myung, N. Kumagai, S. Komaba, H.T. Chung, Solid State Ionics 139 (2001) 47.
[19] W.S. Yoon, K.K. Lee, K.B. Kim, J. Electrochem. Soc. 147 (2000) 2023.
[20] Y. Gao, M.V. Yakovleva, W.B. Ebner, Electrochem. Solid-State Lett. 1 (1998) 117.
[21] J.N. Reimers, E. Rossen, C.D. Jones, J.R. Dahn, Solid State Ionics 61 (1993) 335.
[22] C. Pouillerie, L. Croguennec, C. Delmas, Solid State Ionics 132 (2000) 15.
[23] R.D. Shannon, C.T. Prewitt, Acta Crystallogr. B52 (1969) 925.
[24] C. Pouillerie, L. Croguennec, Ph. Biensan, P. Willmann, C. Delmas, J. Electrochem. Soc. 147 (2000) 2061.
[25] A. Van der Ven, G. Ceder, Meeting Abstracts of Battery Division, 1999 Joint International Meeting, Abstract no. 135, Honolulu, Hawaii, 17–22 October 1999.
[26] A. Van der Ven, G. Ceder, Electrochem. Solid-State Lett. 3 (2000) 301.
[27] M.D. Levi, K. Gamolsky, D. Aurbach, U. Heider, R. Oesten, Electrochim. Acta 45 (2000) 1781.
[28] F. Corse, F. Nobili, A. Deptula, W. Lada, R. Tossici, A.D. Epifanio, B. Scrosati, R. Marassi, Electrochem. Commun. 1 (1999) 605.
[29] Y.M. Choi, S.I. Pyun, S.I. Moon, Solid State Ionics 89 (1996) 43.
[30] M.D. Levi, G. Salitra, B. Markovsky, H. Teller, D. Aurbach, U. Heider, L. Heider, J. Electrochem. Soc. 146 (1999) 1279.